

# MERGERS OF UNEQUAL MASS GALAXIES: SUPERMASSIVE BLACK HOLE BINARY EVOLUTION AND STRUCTURE OF MERGER REMNANTS

FAZEEL MAHMOOD KHAN<sup>1,2</sup>, MIGUEL PRETO<sup>1</sup>, PETER BERCZIK<sup>3,1,4</sup>, INGO BERENTZEN<sup>1,5</sup>, ANDREAS JUST<sup>1</sup>, AND RAINER SPURZEM<sup>3,1,6</sup>

<sup>1</sup>Astronomisches Rechen-Institut, Zentrum für Astronomie, Univ. of Heidelberg, Mönchhof-Strasse 12-14, 69120 Heidelberg, Germany

<sup>2</sup>Department of Physics, Government College University (GCU), 54000 Lahore, Pakistan

<sup>3</sup>National Astronomical Observatories of China, Chinese Academy of Sciences, 20A Datun Rd., Chaoyang District, 100012, Beijing, China

<sup>4</sup>Main Astronomical Observatory, National Academy of Sciences of Ukraine, 27 Akademika Zabolotnoho St., 03680, Kyiv, Ukraine

<sup>5</sup>Heidelberg Institute for Theoretical Studies, Schlosswolfsbrunnenweg 35, 69118 Heidelberg, Germany and

<sup>6</sup>The Kavli Institute for Astronomy and Astrophysics at Peking University (KIAA), Yi He Yuan Lu 5, Hai Dian Qu, Beijing, 100871, China

*Accepted by The Astrophysical Journal*

## ABSTRACT

Galaxy centers are residing places for Super Massive Black Holes (SMBHs). Galaxy mergers bring SMBHs close together to form gravitationally bound binary systems which, if able to coalesce in less than a Hubble time, would be one of the most promising sources of gravitational waves for the *Laser Interferometer Space Antenna* (LISA). In spherical galaxy models, SMBH binaries stall at a separation of approximately one parsec, leading to the “final parsec problem” (FPP). On the other hand, it has been shown that merger-induced triaxiality of the remnant in equal-mass mergers is capable of supporting a constant supply of stars on so-called centrophilic orbits that interact with the binary and thus avoid the FPP. In this paper, using a set of direct  $N$ -body simulations of mergers of initially spherically symmetric galaxies with different mass ratios, we show that the merger-induced triaxiality is also able to drive unequal-mass SMBH binaries to coalescence. The binary hardening rates are high and depend only weakly on the mass ratios of SMBHs for a wide range of mass ratios  $q$ . There is, however, an abrupt transition in the hardening rates for mergers with mass ratios somewhere between  $q \sim 0.05$  and  $0.1$ , resulting from the monotonic decrease of merger-induced triaxiality with mass ratio  $q$ , as the secondary galaxy becomes too small and light to significantly perturb the primary, i.e., the more massive one. The hardening rates are significantly higher for galaxies having steep cusps in comparison with those having shallow cups at centers. The evolution of the binary SMBH leads to relatively shallower inner slopes at the centers of the merger remnants. The stellar mass displaced by the SMBH binary on its way to coalescence is  $\sim 1 - 5$  times the combined mass of binary SMBHs. The coalescence time scales for SMBH binary with mass  $\sim 10^6 M_\odot$  are less than 1 Gyr and for those at the upper end of SMBH masses  $10^9 M_\odot$  are 1-2 Gyr for less eccentric binaries whereas less than 1 Gyr for highly eccentric binaries. SMBH binaries are thus expected to be promising sources of gravitational waves at low and high redshifts.

*Subject headings:* Stellar dynamics – black hole physics – Galaxies: kinematics and dynamics – Galaxy: center.

## 1. INTRODUCTION

Super Massive Black Holes (SMBHs) are now a well established component of galaxies having a sizable bulge (Ferrarese & Ford 2005). In the paradigm of the  $\Lambda$  Cold Dark Matter cosmology, galaxies are formed via hierarchical merging. If more than one of these merging galaxies contain a SMBH, the formation of a binary SMBH is almost inevitable (Begelman et al. 1980). There are cases in which there is a clear observational evidence for two widely separated SMBHs as well as some circumstantial evidence for a true SMBH binary (Komossa 2006). Upon coalescence, SMBH binaries would be the highest signal-to-noise ratio sources of gravitational waves, detectable from essentially any cosmological redshift, for future space-borne gravitational wave detectors such as the *Laser Interferometer Space Antenna* (LISA) (Hughes 2003; Barack & Cutler 2004; Danzmann et al. 2011).

The paradigm for SMBH binary evolution, after a merger of gas-poor galaxies, consists of three distinct phases (Begelman et al. 1980). First, the two SMBHs

sink towards the center due to the dynamical friction exerted by the stars and the dark matter. Dynamical friction acts together with “gravitational slingshot effect” as SMBHs form a bound pair with semi-major axis  $a \sim r_h$ , where  $r_h$  is the binary’s influence radius, which typically is defined to be the radius which encloses twice the mass of the binary in stars  $M(< r_h) = 2M_\bullet$ , where  $M_\bullet$  is the mass of the binary. Dynamical friction stops being an effective driver of inspiral when the binary reaches the *hard binary* separation  $a \sim a_h$  (Quinlan 1996; Yu 2002)

$$a_h := \frac{G\mu_r}{4\sigma^2}, \quad (1)$$

where  $\mu_r$  is the binary’s reduced mass and  $\sigma$  is the 1D velocity dispersion. In the second phase, *slingshot* ejection of stars is the dominant mechanism for taking energy and angular momentum away from SMBH binary. Thirdly, the binary eventually reaches a separation  $a_{\text{GW}}$  at which the loss of orbital energy due to Gravitational Wave (GW) emission drives the final coalescence. The

transition from the first to the second phase is prompt provided that the mass ratio of the remnants is not too small  $q \gtrsim 0.1$  (Callegari et al. 2011). In contrast, the subsequent transition from the second to the third phase could constitute a bottleneck for the binary evolution towards final coalescence caused by lack of stars which can interact with the binary. This is the so-called *Final Parsec Problem*.

Yu (2002) early pointed out, based on an analysis based on the HST sample of nearby elliptical galaxies and spiral bulges from Faber et al. (1997), that flattening and non-axisymmetries would help stellar dynamics in bringing SMBH binaries to coalescence. Merritt & Poon (2004) built self-consistent cuspy, triaxial models with a single SMBH at the center and showed that such models could be concocted with a significant fraction of centrophilic orbits that would efficiently drive the hardening rate of a binary if it were present at the center. Berczik et al. (2006) showed, for the first time with  $N$ -body simulations of rotating King models, that the FPP could potentially be solved by purely stellar dynamical models that develop a significant amount of triaxiality. By including the post-Newtonian ( $\mathcal{PN}$ ) terms into the equations of motion of the binary, Berentzen et al. (2009) explicitly showed that the coalescence times, if the latter models are scaled to real galaxies, are clearly shorter than a Hubble time. Preto et al. (2009) presented preliminary results suggestive that merger-induced triaxiality resulting from the merger of spherically symmetric models would lead to qualitatively similar results – namely the prompt coalescence of resulting SMBH binaries. Khan et al. (2011) (hereafter paper I) and Preto et al. (2011) (hereafter paper II) confirmed and generalized the latter results by showing that galaxies which form via equal mass mergers are mildly triaxial. They have shown that hardening rates of SMBH binaries resulting from equal-mass mergers are substantially higher than those found in spherical nuclei, and are independent of the total number  $N$  of stars, thus allowing them to extrapolate results to real galaxies. Presumably, the nonspherical shapes of merger remnants reported in these studies result in a large population of stars on centrophilic orbits. Inside the influence radius of SMBH, the centrophilic orbit family includes saucer or cone orbits in the axisymmetric potentials (Sridhar & Touma 1999) and pyramids orbits (angular momentum close to zero) in triaxial potentials (Merritt & Vasiliev 2011). Outside the influence radius, most of the centrophilic orbits are chaotic in a triaxial potential (Poon & Merritt 2001).

The inspiral of a binary SMBH is expected to leave a characteristic imprint in the morphological and dynamical properties of the newly formed galactic nucleus following the merger: e.g., the bending and precession of radio jets (Roos et al. 1993), the variability in optical light curve of quasar (Valtonen et al. 2008), X-shaped radio lobes (Merritt & Ekers 2002) and, with some likelihood, a partially depleted core instead of a steep cusp in bright elliptical galaxies (Graham 2004; Kormendy et al. 2009) could be explained by different models of SMBH binary evolution prior or after coalescence (Merritt et al. 2007; Gualandris & Merritt 2008).

Detailed surface photometry of ellipticals has revealed that their surface brightness is well described by a Sérsic

profile,  $\log I(r) \propto r^{1/n}$ , over most of the body of a bulge or early-type galaxy. However, systematic deviations from this profile are found in the innermost regions close to the central SMBH – either in the form of a light (mass) excess or deficit with respect to that would result from the extrapolation of the Sérsic profile towards the center (Kormendy et al. 2009). In other words, observations seem to reveal a dichotomy in the central density profiles of bulges and early-type galaxies: giant, high-luminosity objects have relatively shallow central density profiles while normal, low-luminosity ones show steeper density profiles in their center. The former are often called *core* galaxies and show density profiles with central logarithmic slopes  $\gamma < 1$ , and typically harbor SMBH of mass  $\gtrsim 10^8 M_\odot$ ; while the latter are normally called *power law* galaxies, have central  $\gamma > 1$  and lighter SMBH  $\lesssim \text{few} \times 10^7 M_\odot$ . The explanation of cores is non-trivial since dry mergers should preserve the highest density in phase space given that, by virtue of being devoid of appreciable amounts of gas, their dynamics is essentially collisionless (Binney & Tremaine 2008).

Galaxies having a single mass stellar population are expected to have Bahcall & Wolf (1976) cusp around the SMBH with  $\rho(r) \propto r^{-\alpha}$ ,  $\alpha \sim 7/4$  for  $r \lesssim r_h$  after a relaxation time (Preto et al. 2004). In the more realistic case where there is a range of stellar masses, less massive objects follow a shallow profile,  $\alpha \sim 3/2$ , while heavier objects (e.g. stellar black holes) develop steeper cusps  $\alpha \sim 2$  around the SMBH (Bahcall & Wolf 1977; Alexander & Hopman 2009). Whether a given, or the typical, nucleus has reached this relaxed state or not depends on its “initial” profile and on how long ago it was formed. Different studies have reached different conclusions regarding the most probable state of the stellar distribution around the SMBH after a relaxation time. Preto & Amaro-Seoane (2010), who performed Fokker-Planck and  $N$ -body simulations of a two component galaxy nucleus model made of solar mass stars and stellar mass black holes, obtained mass-segregated stellar cusps in  $\sim 1/4$  of a relaxation time. However, Gualandris & Merritt (2012) state roughly the opposite conclusion: that even after a few central relaxation times, the distribution of stars can be very different than in the steady-state, mass-segregated solutions.

The analysis of the number counts of spectroscopically identified, old stars in the sub-parsec region of our own Milky Way (Buchholz et al. 2009; Do et al. 2009) seems to favor the presence of a very shallow profile for the *visible* fraction of the old stellar population. This is consistent with the finding that the two-body relaxation time at the influence radius of the SMBH in the center of the Milky Way is longer than a Hubble time (Merritt 2010; Preto & Amaro-Seoane 2010). On the other hand, low-luminosity spheroids often contain nuclear star clusters which have central relaxation times shorter than a Hubble time (Merritt 2009).

In dry mergers, i.e. in the absence of a dynamically significant amount of gas, the slingshot ejection of stars by the central SMBH binary drives the binary inspiral. It has early been proposed that inspiraling binaries could carve a core inside  $\sim r_h$ , thus providing an explanation for the mass deficits present in the center of gas-poor giant ellipticals (Makino & Ebisuzaki 1996). On energetic grounds it can be shown that in order for the binary to

reach coalescence, it needs to eject an amount of stellar mass of order of its own mass,  $M_{\text{ej}} \sim \alpha \times M_{\bullet}$ , where  $\alpha = O(1)$  and  $M_{\bullet} = M_{\bullet,1} + M_{\bullet,2}$  (Merritt & Milosavljević 2005; Perets & Alexander 2008). Merritt (2006a) studied the mass deficits created by SMBH inspirals evolving in spherical symmetric nuclei and found an average  $\alpha \sim 0.5$ . However, unless their mass  $M_{\bullet} \lesssim \text{few} \times 10^6 M_{\odot}$ , the evolution of SMBH binaries in gas-poor *spherical* galaxies tends to stall due to depletion, on the (local) dynamical timescale, of the pool of stars whose orbits intersect the binary (e.g. Milosavljević & Merritt 2003; Makino & Funato 2004; Berczik et al. 2005; Khan et al. 2011; Preto et al. 2011). The binaries studied by Merritt (2006a) did not reach coalescence due to the FPP. Therefore they estimated mass deficits at the time when a hard binary forms in their simulations. Merritt et al. (2007) extended the latter study by following the inspiral of binaries up to coalescence in the lower mass range using an approximate Fokker-Planck description for stellar scattering. They find substantially higher mass deficits than before, albeit restricting their calculations to spherical models and very shallow cusps (with initial  $\gamma \sim 1/2$ ) in strong contrast with the larger  $\gamma$  typical of compact low-mass nuclei. More precise estimates of  $\alpha$  from more realistic galaxy merger studies are therefore certainly needed; in particular, ones that do not rely on any of the following approximations: spherical symmetry, low  $\gamma$ , crude model for inferring the mass ejected from the increase in the binary’s orbital energy, or those generally inherent to the Fokker-Planck formalism. In this respect, preliminary studies of mass deficits created by the merger of equal mass galaxies, with moderate SMBH mass ratio, moderate central slope  $\gamma \sim 1$ , and that generate mildly triaxial remnants, suggest that the resulting mass deficits could be substantially higher  $M_{\text{ej}} \sim 2M_{\bullet}$  within  $\lesssim 3r_{\text{h}}$  (Preto et al. 2009) – a result which we confirm and generalize in this paper. Note, however, that alternative scenarios for explaining the formation of cores have been proposed (Gualandris & Merritt 2008).

In this paper, we revisit these problems by detailed  $N$ -body simulations using a range of more realistic models of merging galactic nuclei with varying mass ratio  $q$  and central logarithmic slopes  $\gamma$ . We restrict the simulations to  $q = M_{\text{gal},s}/M_{\text{gal},p} = M_{\bullet,2}/M_{\bullet,1}$ . We study the shape of the merger remnant of galaxies having different density profiles and different mass ratios. For each of our models, the hardening rate of the SMBH binary, the axis ratios of the merger remnant and the resulting mass deficit are calculated. In section 2, we describe our initial models and numerical methods used in our study. The evolution of SMBH binary in galaxy mergers is described in section 3, as well as the time evolving densities and shapes of newly formed galaxies resulting from the galaxy merger. Section 4 describes the analysis and results of “mass-deficits” resulting from the galaxy mergers. The coalescence timescales for binary SMBHs from the time of formation of binary till the full coalescence of SMBHs due to emission of gravitational waves are presented in section 5. Finally, section 6 summarizes and discusses the results of the paper.

## 2. INITIAL CONDITIONS AND NUMERICAL METHODS

### 2.0.1. The host galaxies and their SMBHs

Our aim is to study the dependence of the hardening rates with the mass ratios and central concentration of the nucleus – as well as the resulting imprint of the SMBH inspiral on the stellar distributions of post-coalescence nucleus. Following closely the initial set-up of our previous numerical experiments (see papers I and II), we represent the individual galaxies or galactic nuclei by spherically symmetric  $N$ -body models. The density profile of the models follows the Dehnen (1993) profile of the form

$$\rho_{\text{D}}(r) = \frac{(3 - \gamma)M_{\text{gal}}}{4\pi} \frac{r_0}{r^{\gamma}(r + r_0)^{4-\gamma}}, \quad (2)$$

where  $M_{\text{gal}}$  is the total mass of the galaxy,  $r_0$  is the scale radius, and  $\gamma$  is the inner logarithmic slope. For  $r \gg r_0$ , the density declines with a logarithmic slope of  $-4$ , which, although not close to the exterior density of real galaxies, provides a convenient cut-off that avoids the waste of CPU time in following stars whose orbits are too far from the SMBH binary to have any significant impact on its long term evolution. The resulting cumulative mass profile is given by

$$M_{\text{D}}(r) = M_{\text{gal}} \left( \frac{r}{r + r_0} \right)^{3-\gamma}. \quad (3)$$

In addition, we represent the SMBHs by massive particles with zero velocity placed at the center of both the primary and the secondary galaxies. The masses of the SMBHs are set to be 0.5 percent of their host galaxy. This value is few times higher than the currently accepted value of  $M_{\text{gal}}/M_{\bullet} \sim 0.001$  (Ferrarese & Merritt 2000; Gebhardt et al. 2000; Merritt & Ferrarese 2001; Häring & Rix 2004). However, some galaxies may have larger value of this ratio than others.

Thus the two SMBHs in the simulations have the same mass ratio  $q$  as their host galaxies. The Dehnen models have an isotropic distribution function of velocities (no net rotation), are spherically symmetric and are initially set-up to be in dynamical equilibrium with a gravitational potential given by  $\Phi(r) = -GM_{\bullet}/r + \Phi_{*}(r)$ , where  $\Phi_{*}(r)$  is the gravitational potential due to the stars alone.

The galaxies size ratio scales with the corresponding mass ratio as  $R_2/R_1 \propto \sqrt{M_2/M_1}$ . By choosing four different values of  $\gamma = 0.5, 1.0, 1.5, 1.75$ , the central part of our galaxy models represent the variety of observed density profiles in both early and late type galaxies.

For Dehnen models the ratio of the effective radius (projected half-mass radius)  $R_{\text{e}}$  to the half-mass radius  $r_{1/2}$  is given approximately as

$$\frac{R_{\text{e}}}{r_{1/2}} \approx 0.75, \quad (4)$$

and shows only a weak dependence on  $\gamma$ . In the following we refer to the more massive galaxy as the *primary* galaxy and the lighter one as the *secondary*. In our model units we use for our primary galaxy a total mass and scale radius of  $M_{\text{gal},p} = r_{0,p} = 1$ . We also set the gravitational constant to  $G = 1$ .

In the absence of relativistic effects on the binary’s orbit, our models are scale-free and can be *a posteriori* scaled to galaxies of different total mass and size. However, the inclusion of radiation reaction effects on the

TABLE 1  
MODEL PARAMETER AND PROPERTIES OF THE PRIMARY GALAXY.

| Model | $N$  | $\gamma$ | $r_{1/2}$ | $R_{\text{eff}}$ |
|-------|------|----------|-----------|------------------|
| A     | 128k | 0.5      | 3.13      | 2.35             |
| B     | 128k | 1.0      | 2.41      | 1.81             |
| C     | 128k | 1.5      | 1.69      | 1.27             |
| D     | 64k  | 1.75     | 1.35      | 1.01             |

NOTE. — Columns from left to right show the model name, the particle number  $N$ , the half-mass radius  $r_{1/2}$  and the effective radius  $R_{\text{eff}}$ , respectively, for our primary galaxy models.

binary due to GW emission introduces an absolute scale associated to the universal value of the speed of light. Such scalings are described in detail in section 5 when coalescence times are explicitly computed.

The effective radii of our models can be compared to the effective radii in observed galaxies to calculate  $r_0$ . By fixing galaxy mass  $M_{\text{gal}}$  our models can be scaled to physical units using following relations:

$$[T] = \left( \frac{GM_{\text{gal,p}}}{r_{0,p}^3} \right)^{-1/2} = 1.5 \text{Myr} \left( \frac{M_{\text{gal,p}}}{10^{11} M_{\odot}} \right)^{-1/2} \left( \frac{r_{0,p}}{\text{kpc}} \right)^{3/2}, \quad (5)$$

$$[V] = \left( \frac{GM_{\text{gal,p}}}{r_{0,p}} \right)^{1/2} = 655 \text{km s}^{-1} \left( \frac{M_{\text{gal,p}}}{10^{11} M_{\odot}} \right)^{1/2} \left( \frac{r_{0,p}}{\text{kpc}} \right)^{-1/2}. \quad (6)$$

We have performed a series of  $N$ -body experiments where we vary the mass ratio of the galaxies and SMBHs  $q$  and the inner density slope  $\gamma$ . In Table 1 we summarize the model parameters and properties for the primary galaxies used in our simulations. The computational wallclock time increases with increasing cuspsiness (higher  $\gamma$ ) of the density profile since particles in the center need very small numerical timesteps in order to resolve accurately the (locally) strongly varying gradients of the gravitational potential. In order to keep the computational time within reasonable limits we built our model D (highest  $\gamma = 7/4$ ) with only half as many particles as the other models.

The secondary galaxies used in our merger simulations have the same density profile, i.e., the same  $\gamma$ , as the primary galaxies, but have different masses  $M_{\text{gal,s}}$  and scale radii  $r_{0,s}$ . Both primary and secondary galaxy models have equal number of particles  $N$ .

The initial center of mass positions and velocities for the two galaxies are calculated from the Keplerian orbit of the equivalent two-body problem, with given apo- and peri-centers,  $r_a$  and  $r_p$ , respectively. The two galaxies start at the apo-center of their relative orbit. The initial separation between the center of mass of the two galaxy is  $\Delta r = 15r_{0,p}$ ; and since the half-mass radius of each nucleus is  $R_{1/2} \lesssim 2.5$ , this choice ensures that the galaxies are initially well separated while, at the same time, we minimize computing time. The initial relative velocity of the two galaxies is chosen such that the SMBH separation at first peri-center passage is  $\sim 2r_{0,p}$ ; in other

TABLE 2  
PARAMETERS OF THE GALAXY MERGERS STUDY

| Run | $N_{\text{tot}}$ | $\gamma$ | $q$  | $r_{0,s}$ |
|-----|------------------|----------|------|-----------|
| A1  | 256k             | 0.5      | 0.1  | 0.316     |
| A2  | 256k             | 0.5      | 0.25 | 0.5       |
| A3  | 256k             | 0.5      | 0.5  | 0.707     |
| A4  | 256k             | 0.5      | 1.0  | 1.0       |
| B1  | 256k             | 1.0      | 0.1  | 0.316     |
| B2  | 256k             | 1.0      | 0.25 | 0.5       |
| B3  | 256k             | 1.0      | 0.5  | 0.707     |
| B4  | 256k             | 1.0      | 1.0  | 1.0       |
| B5  | 256k             | 1.0      | 0.05 | 0.22      |
| C1  | 256k             | 1.5      | 0.1  | 0.316     |
| C2  | 256k             | 1.5      | 0.25 | 0.5       |
| C3  | 256k             | 1.5      | 0.5  | 0.707     |
| C4  | 256k             | 1.5      | 1.0  | 1.0       |
| D1  | 128k             | 1.75     | 0.1  | 0.316     |
| D2  | 128k             | 1.75     | 0.25 | 0.5       |
| D3  | 128k             | 1.75     | 0.5  | 0.707     |
| D4  | 128k             | 1.75     | 1.0  | 1.0       |

NOTE. — Col.(1) Galaxy merger model. Col(2) Number of particles. Col(3) Central density profile index  $\gamma$ . Col(4) Mass ratio of merging galaxies and their black holes. Col(5) Scale radius of secondary galaxy.

words, the initial orbit of the binary galaxy has eccentricity  $\sim 0.75$ , which corresponds to a circularity parameter value of  $\epsilon = L/L_c \sim 0.66$  in rough agreement with the values measured from full galaxy scale merger simulations (Kazantzidis 2010).

## 2.1. Numerical Methods and Hardware

The  $N$ -body integrations are carried out using the  $\phi$ GRAPE<sup>1</sup> (Harfst et al. 2007), a parallel, direct-summation  $N$ -body code that uses general purpose hardware, namely Graphic Processing Units (GPU) cards to accelerate the computation of pairwise gravitational forces between all particles. Our updated version of the  $\phi$ GRAPE (= **P**arallel **H**ermite **I**ntegration with **G**RAPE) code uses the 4-th order Hermite integration scheme to advance all particles with hierarchical individual block time-steps, together with the parallel usage of GPU cards to calculate the acceleration  $\vec{a}$  and its first time derivative  $\dot{\vec{a}}$  between all particles. For the force calculation we use the SAPPORO (Gaburov et al. 2009) library which emulates on the GPU the standard GRAPE-6 library calls.

As  $\phi$ GRAPE does not include the regularization (Mikkola & Aarseth 1998) of close encounters or binaries, we have to use a gravitational (Plummer-)softening between all components. The softening length is chosen to be sufficiently small (i.e.  $5 \times 10^{-5}$  in our model units) to keep the (dense) stellar system as collisional as possible/necessary. In the few runs in which we include the  $\mathcal{PN}$  terms to the equations of motion of the SMBH binary, the softening between the SMBH particles is set equal to zero. Our implementation of the  $\mathcal{PN}$  terms is identical to that used in Berentzen et al. (2009), except that we cut-off the  $\mathcal{PN}$  expansion at the next order. We stress that the binary is, in all cases, integrated taking into account the gravitational field from the stellar cluster.

The  $N$ -body integrations were carried out on three

<sup>1</sup> <ftp://ftp.ari.uni-heidelberg.de/staff/berczik/phi-GRAPE/>

computer clusters. “titan”, at the Astronomisches Rechen-Institut in Heidelberg, the GPU-enhanced cluster “kolob” at the University of Heidelberg and “laohu” in Beijing.

For a detailed discussion on the  $N$ -body methods and choice of parameters, we refer the reader to paper I.

### 3. SMBH BINARY EVOLUTION IN GALAXY MERGERS

Figure 1 shows the relative separation  $R$  between the two black holes during a galaxy merger. According to the equivalent two-body trajectory used to set up the initial galaxy orbital parameters, the galaxy centers, and hence the SMBHs, should reach a separation of  $2r_{0,p}$  during the first pericenter passage. However, as figure 1 shows, in case  $q \gtrsim 1/2$ , the SMBH separation shrinks well below  $2r_{0,p}$  during the galaxy merger phase. As  $q$  decreases, and hence the mass of the secondary galaxy decreases as well, the galaxies reach the first pericenter passage after following more closely the corresponding two-body orbit. In the same figure the color of the arrows signals the time  $T$  at which the two SMBHs in a particular model form a binary system. As  $q$  decreases, the arrows move from left to right signaling the longer interval of time between the start of merger and formation of the binary. Neither the time  $T$  nor  $R_{\text{peri}}$  are as sensitive to  $\gamma$  as they are to  $q$ .

When the SMBHs become bound their separation is  $R \approx r_h$ . Once a SMBH binary is formed, dynamical friction and the ejection of stars by the gravitational slingshot, act together to efficiently extract angular momentum from the massive binary and the binary separation shrinks rapidly. When the semi-major axis  $a \approx a_h$ , this initial rapid phase of binary hardening comes to an end as the pool of stars whose orbits cross the binary orbit gets depleted on the (local) dynamical timescale.<sup>2</sup>

The subsequent hardening of the binary occurs only if the loss cone orbits are replenished.<sup>3</sup> In a spherical galaxy with no gas, the only dynamical mechanism for replenishing loss cone orbits is two-body relaxation, with the corresponding timescale for repopulating the loss cone orbits scaling as  $\sim N/\ln N$  (Binney & Tremaine 2008), and the inspiral rate thus becomes strongly  $N$ -dependent (Makino & Funato 2004; Berczik et al. 2005). In papers I and II, it was shown that the hardening phase, in the case of a mildly triaxial remnant nuclei resulting from a galaxy merger, is essentially  $N$ -independent – which allows our results to be scaled to real galaxies whose typical number of stars,  $N_{\text{star}}$ , is always several orders of magnitude larger than the maximum number reachable with state-of-the-art direct  $N$ -body simulations. Furthermore, it was also shown in Papers I & II that the flux of stars into the loss cone in a triaxial remnant is also consistently higher than in the spherical case, meaning the binary evolution and coalescence can occur much faster than in spherical models.

Figure 2 shows the time evolution of the binary’s inverse semi-major axis  $1/a$  from the time  $T$  when the two

black holes become bound. An initial phase with faster binary hardening becomes more evident for steep inner density profiles ( $\gamma = 1.5, 1.75$ ) – presumably corresponding to the clearing of the original loss cone (Yu 2002). The binary hardening rates  $s$  are calculated by fitting straight lines to  $a^{-1}(t)$  in the late phase of binary evolution from  $T = 60 - 100$ . The results are shown in Figure 3. The hardening rates depend very weakly on the mass ratio of binary SMBHs, in contrast with the  $\sim M_\bullet$  dependence found in equal mass merger study (papers I & II) and, for fixed  $M_\bullet$ , on the mass ratio  $q$ . On the other hand, the value of  $s(t)$  increases significantly for higher values of  $\gamma$ . Note that for the single run with the smallest mass ratio in our sample,  $q = 0.05$  and  $\gamma = 1$ , the hardening rates are significantly weaker than the remaining  $\gamma = 1$  models.

Following Paper II, the SMBH binary hardening rate, which is a measure for the energy loss of the binary, is given by

$$s(t) \equiv \frac{d}{dt} \left( \frac{1}{a} \right) \approx \frac{2m_* \langle C \rangle}{M_\bullet a} \int_0^{+\infty} dE \mathcal{F}_{lc}(E, t), \quad (7)$$

where  $\mathcal{F}_{lc}(E, t)$  is stellar flux into the loss cone,  $\langle C \rangle = O(1)$  is a dimensionless quantity obtained from three-body scattering experiments (Quinlan 1996) and  $E = GM_\bullet/r + \Phi_*(r) - 1/2 v^2$  is the (specific) energy of each star ( $E > 0$  for bound stars). The behavior of the hardening rates can thus be qualitatively understood as follows. The flux  $\mathcal{F}_{lc}(E, t)$ , and its time evolution, depends on the degree of symmetry in the underlying gravitational potential (or, equivalently, the orbit families supported by it) – including the radial density distribution of stars around the binary. On the other hand, the flux of stars into the loss cone is expected to peak around  $r_h$  (Perets & Alexander 2008). For a given energy  $E$  and fixed  $M_\bullet$ ,  $\mathcal{F}_{lc}(E, t) \propto n(E, t)/\tau(E, t)$  where  $n(E, t)$  is the number of stars of energy  $E$  per unit (specific) energy, while  $\tau(E, t)$  is equal, in the spherical case, to  $\tau_{\text{rlx}} \propto \sigma^3/\rho \propto r\gamma^{-3/2}$  (Binney & Tremaine 2008) or, in the triaxial case, to the star’s orbital precession time  $\tau_{\text{prec}}(E, t) \propto M_*^{-1/2}(< r) \propto r^{(3-\gamma)/2}$ , for  $r \lesssim \text{few} \times r_h$  (Yu 2002). Note that, for typical nucleus parameters,  $\tau_{\text{prec}} \ll \tau_{\text{rlx}}$ . As a result, and since for more concentrated nuclei (higher  $\gamma$ )  $n(E_h, t)$  is higher and  $\tau(E, t)$  is shorter, so more concentrated nuclei experience higher  $\mathcal{F}_{lc}$  and higher  $s(t)$ .

The triaxiality also plays an important role in determining the hardening rate. This is because of its role in supporting centrophilic orbits; in fact, at fixed  $n(E, t)$  only a fraction of the stars will be on centrophilic orbits, and this fraction is an increasing function of increasing triaxiality. As  $q$  decreases, the triaxiality of the remnant also decreases as shown in Figure 4. This results presumably in a weaker hardening rate since the fraction of stars on centrophilic orbits is smaller. This effect partially explains why the dependence of the hardening rate on  $M_\bullet$  is much weaker than expected based on the results obtained in Papers I and II for equal-mass mergers.

We analyze the shape of the merger remnant by calculating principal axis ratios and density profiles for galaxy merger models. Figure 4 shows the principle axis ratios of the merger remnant; these were defined as the axis ratios of a homogeneous ellipsoid with the same in-

<sup>2</sup> The semi-major axis  $a$  and eccentricity  $e$  of the binary are defined here via the standard Keplerian relations, i.e., neglecting effects of the field stars.

<sup>3</sup> The loss cone is the region of phase space corresponding, roughly speaking, to orbits that cross the binary, i.e. with angular momentum  $J \lesssim J_{lc} = \sqrt{GM_\bullet f a_{\text{bin}}}$ , where  $f = \mathcal{O}(1)$  (Lightman & Shapiro 1977).

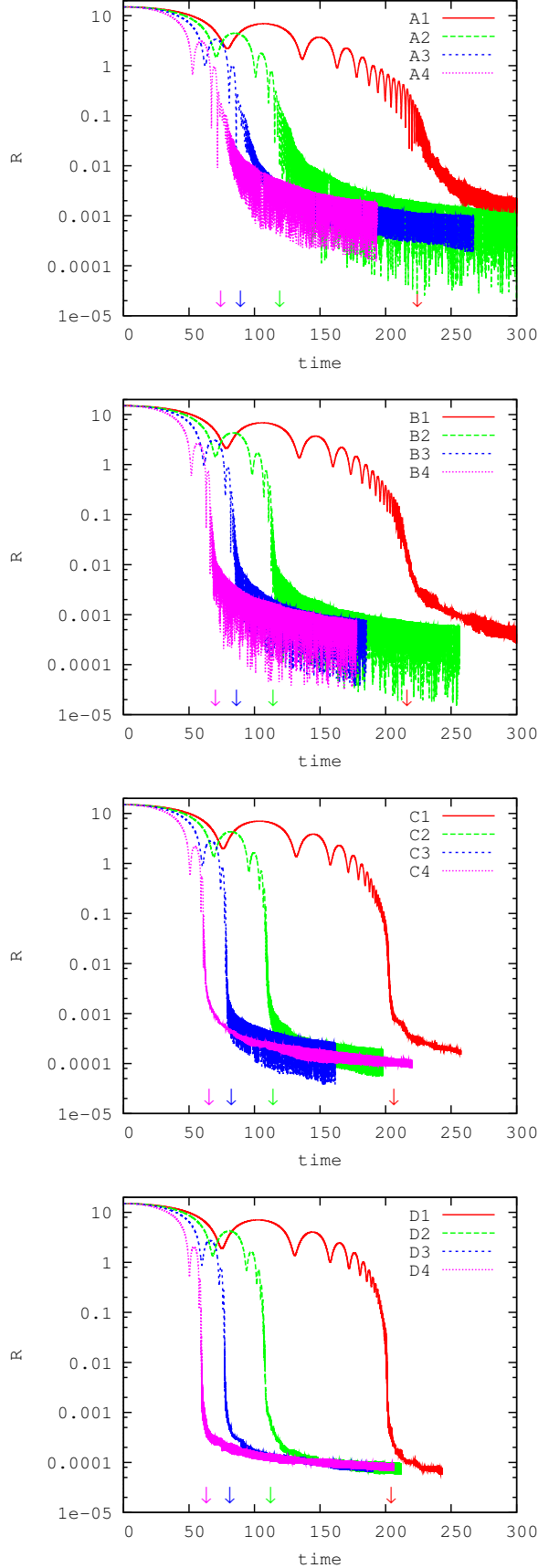


FIG. 1.— Evolution of the separation between the SMBHs, in  $N$ -body integrations of galaxy mergers for  $\gamma = 0.5, 1.0, 1.5$  and  $1.75$  (top to bottom) according to Table 2. The arrows represent the time ( $T = 0$ ) at which the two black holes become gravitationally bound for each model. Time and  $R$  are measured in  $N$ -body units.

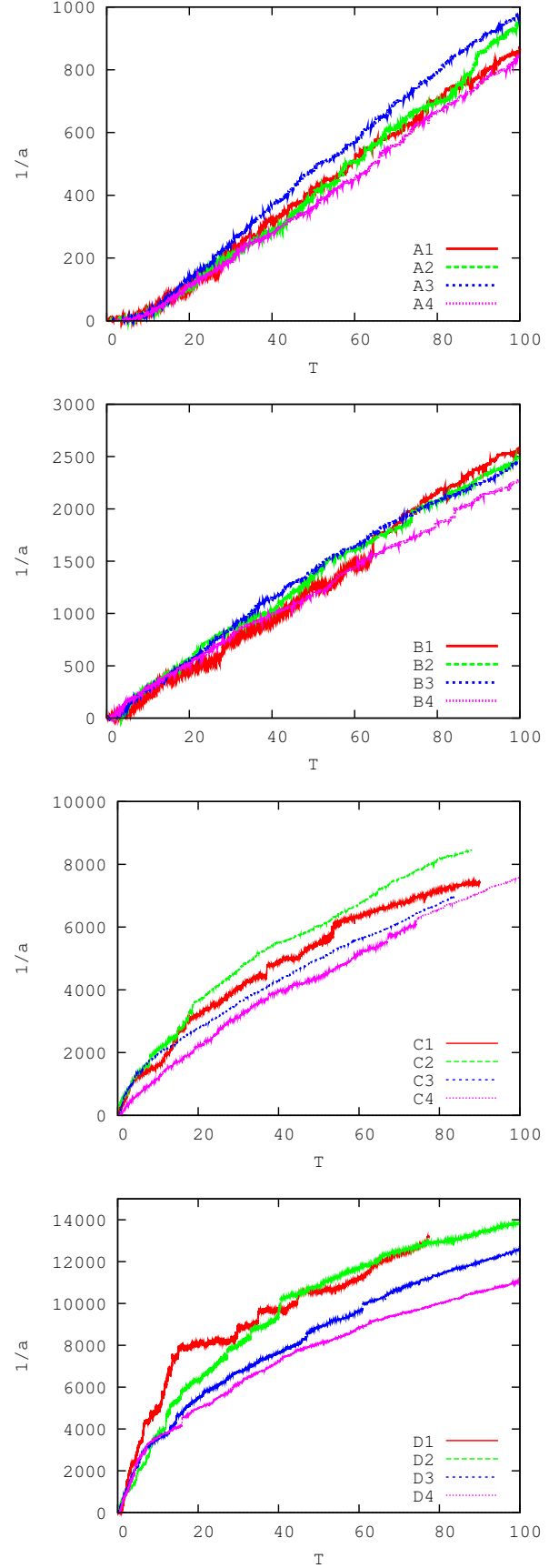


FIG. 2.— Evolution of SMBH binary semi-major axis, in  $N$ -body integrations of galaxy mergers for  $\gamma = 0.5, 1.0, 1.5$  and  $1.75$  (top to bottom) according to Table 2.  $T$  measures the time since the instant when the SMBHs formed a bound pair.

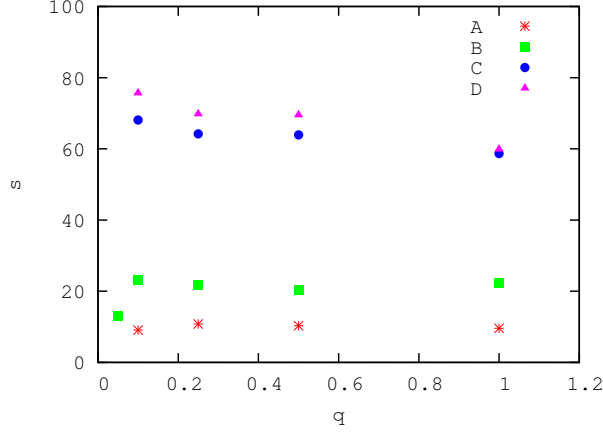


FIG. 3.— Average hardening rates for  $\gamma = 0.5, 1.0, 1.5$  and  $1.75$  according to Table 2. The average is measured between  $T = 60$  and  $T = 100$  in  $N$ -body units. See text for details.

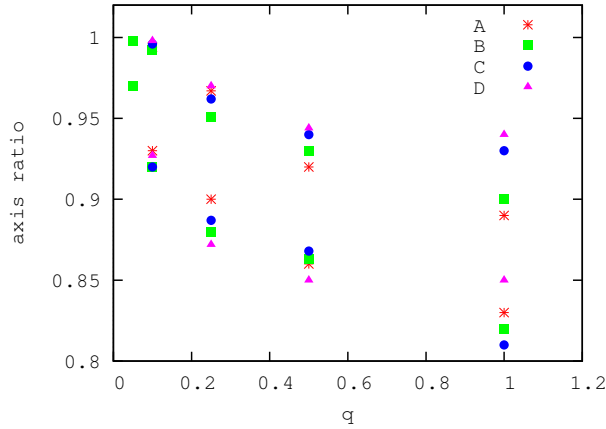


FIG. 4.— Ratio of intermediate to major ( $b/a$ , upper series of points) and minor to major ( $c/a$ , lower series of points) axes for  $\gamma = 0.5, 1.0, 1.5$  and  $1.75$  according to Table 2.

ertia tensor. The departures from spherical symmetry become more apparent for mergers with larger  $q$ . For  $q = 0.05$  and  $0.1$ , the merger-induced triaxiality becomes residual and the remnant results only a slightly flattened system. The dynamical effect of this transition seems to be abrupt, as the hardening rates shown in Figure 3 are essentially independent of mass ratio down to  $q \sim 0.1$ . In such minor mergers, the secondary galaxy gets tidally disrupted within a few pericenter passages, and eventually the *naked* black hole of satellite spirals in due to dynamical friction. The evolution of SMBH binary in such a merger results very similar to those of binaries embedded in spherical galaxy models. Nevertheless in reality situations such as these are not very likely to happen as both galaxies would surely retain some triaxiality or flattening from a previous major merger.

The density profiles of the newly formed galaxies as the result of the merger are shown in figure 5. As a result of the galaxy merger and the ejection of stars from the central galaxy region by the inspiraling black holes, the merger remnant nuclei have significantly shallower inner slopes than those of its progenitors. The "damage" caused by in-falling black holes increases with their mass. The values of  $\gamma_f$  are calculated by fitting Dehnen's model

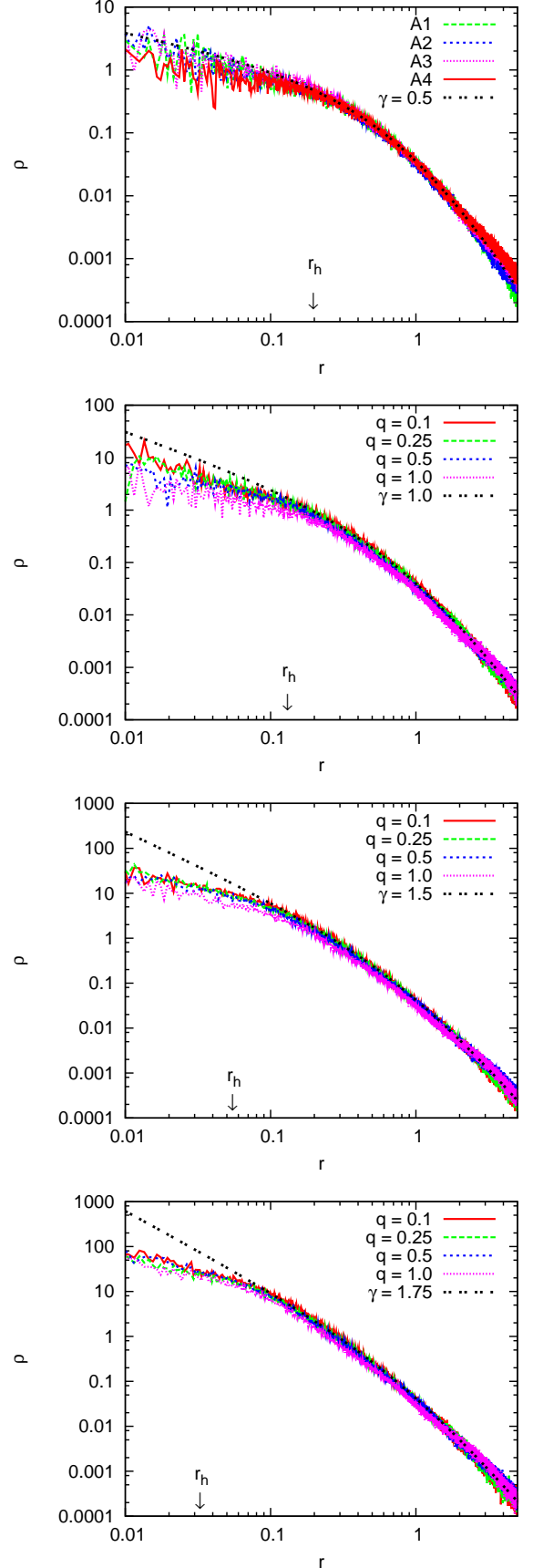


FIG. 5.— Density profiles of merger remnant for  $\gamma = 0.5, 1.0, 1.5$  and  $1.75$  (top to bottom) according to Table 2.



to merger remnant right after the time when phase of rapid binary hardening ends. Table 3 presents the final inner slopes for merged galaxies.

#### 4. MASS DEFICITS

Observations of nearby galaxies show that Sérsic functions provide remarkably accurate fits for the major axis brightness surface profiles over the main bodies of bulges and early-type galaxies. This has been confirmed with increased accuracy and dynamic range over the last decade or so (Kormendy et al. 2009). Moreover, detailed state-of-the-art simulations of merging galaxies also generate profiles which are consistent with Sérsic functions (Hopkins et al. 2009a,b). Even though there is not a complete theoretical understanding for the remarkable regularity of these profiles, their apparent generality and robustness led people to identify and interpret departures from Sérsic fits and use them as a probe of the physics underlying the co-evolution of galaxies and their massive black holes.

Cores tend to be found in giant ellipticals and are loosely defined as the central region in a bulge or early-type galaxy where the surface brightness deviates and it is below the values that would result from the extrapolation of the Sérsic profile from the main body of the object down to its innermost region. Typically they are associated to shallower cusps with  $\gamma \lesssim 0.5 - 1$ . One possible explanation of a central core in a gas poor galaxy can be attributed to the ejection of stars by a hard SMBH binary. The destruction caused by the inspiraling massive black hole in the center of galaxy can be measured in-terms of missing mass called “mass-deficit”. Graham (2004) and Ferrarese et al. (2006) measured the mass-deficits from the difference in flux between the observed galaxies light profiles at the center and the inward extrapolation from their outer Sérsic profiles. Estimated mass-deficits from these studies yield  $M_{\text{def}} \sim (1 - 2)M_{\bullet}$ , and values as high as  $\sim (4 - 5)M_{\bullet}$  were uncommon. More recent studies obtained larger values with an average value  $\langle M_{\text{def}}/M_{\bullet} \rangle \sim 11$  and an error in the mean of about 18% (Kormendy et al. 2009).

Top panel of figure 6 shows the cumulative mass profile for model C1 at different time of its evolution. The merger of a secondary galaxy with the primary causes some changes in the inner profile of the latter. This can be seen by comparing the profiles at times  $t = 0$  and  $t = 100$ , between which there is a noticeable drop in the stellar density around  $r_h$  due to the merging of the two galaxies. Then, as the secondary is being tidally disrupted, after a few pericenter passages, the profile of the resulting merger remnant remains stable. Once, at time  $t \sim 202$ , the two black holes become bound and form a binary, the stars inside the loss cone start to be cleared by the binary and a rapid evolution of the mass profile ensues till  $t \sim 240$ . This drop in the central density is due to the slingshot ejection of stars by the binary. As a result, the the mass inside  $\sim \text{few} \times r_h$  drops rapidly hence changing the mass-profile there. Once this phase of rapid mass ejection ends, the density profile – notably inside  $r_h$  – remains almost constant as the binary continues its inspiral. This can be understood as follows. Inside  $r_h$ , the gravitational potential is approximately spherical and thus the stars residing there can enter the loss cone only by diffusing in energy and angular mo-

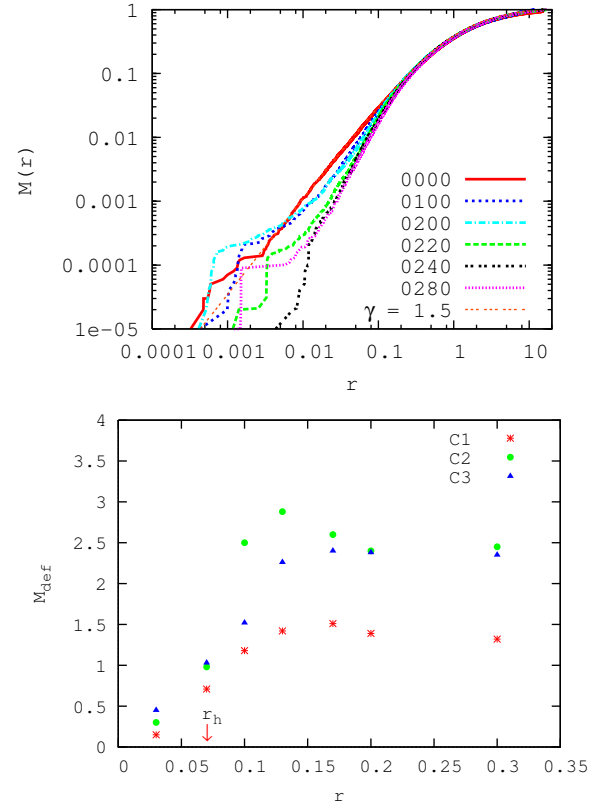


FIG. 6.— Cumulative mass profile for one of our merger models at different time steps (top) and mass deficits normalized to  $M_{\bullet}$  for models C (bottom). Central density profiles at the beginning ( $t = 0$ ) and end ( $t = 280$ ) are  $\gamma = 1.5$  and  $\gamma \sim 1$ , respectively. The red arrow in the bottom panel of the figure shows the influence radius at the time of the formation of the SMBH binary.

mentum space through two-body encounters. The corresponding timescale is the relaxation time which scales as  $\tau_{\text{rlx},J} \sim \sigma^3/\rho \sim r^{\gamma-3/2}$  (Spitzer 1987); since  $\gamma \lesssim 3/2$  for all models at almost all times of interest, this implies that  $\tau_{\text{rlx}}$  increases towards the center. The timescale for such stars to enter the loss cone is thus much longer than the typical precession time needed for centrophilic orbits of stars, resident at distances  $\gtrsim r_h$ , to come sufficiently close to interact with the binary. As a result, the density profiles well inside  $r_h$  remain essentially constant during the remainder of the inspiral so the damage impinged on the cusp by the SMBH inspiral following a merger is less severe than naive spherical model scenarios might let expect. The conclusion is that it is not very likely that a hole in the stellar distribution will ever be created by such mergers.

We calculate the mass-deficits for each of our galaxy mergers as the difference between the stellar mass enclosed at a given radius at the time when the binary becomes bound and at the end of the runs. The end of the run is *a priori* a somewhat arbitrary choice since not all runs end at exactly the same point in the binary’s inspiral. However, when we compare the four cases (A2, A4, B3 and B4) for which we followed the binary up to final coalescence, we realize that most of the change in the density profiles happens at a relatively early stage in



TABLE 3  
MASS DEFICIT ANALYSIS

| Run                  | $r_h$ | $\gamma_f$ | $a_{\text{final}}$    | $T_{\text{final}}$ | $M_{\text{def},1}$ | $M_{\text{def},1.5}$ | $M_{\text{def},2}$ | $M_{\text{def},2.5}$ | $M_{\text{def},3}$ |
|----------------------|-------|------------|-----------------------|--------------------|--------------------|----------------------|--------------------|----------------------|--------------------|
| A1                   | 0.19  | 0.34       | $6.4 \times 10^{-4}$  | 180                | 0.51               | 0.76                 | 0.84               | 0.93                 | 0.72               |
| A2                   | 0.19  | 0.26       | $5.5 \times 10^{-4}$  | 180                | 0.50               | 0.94                 | 1.20               | 1.20                 | 1.05               |
| A2( $\mathcal{PN}$ ) | 0.19  | 0.23       | <i>merged</i>         | 160                | 0.48               | 0.91                 | 1.11               | 1.14                 | 1.01               |
| A3                   | 0.19  | 0.22       | $5.9 \times 10^{-4}$  | 210                | 0.68               | 1.21                 | 1.49               | 1.40                 | 1.34               |
| A4                   | 0.22  | 0.18       | $9.7 \times 10^{-4}$  | 220                | 0.58               | 0.76                 | 1.05               | 1.50                 | 1.86               |
| A4( $\mathcal{PN}$ ) | 0.22  | 0.15       | <i>merged</i>         | 204                | 0.59               | 0.74                 | 1.06               | 1.47                 | 1.81               |
| B1                   | 0.155 | 0.61       | $2.9 \times 10^{-4}$  | 140                | 0.50               | 1.18                 | 1.31               | 1.38                 | 1.64               |
| B2                   | 0.14  | 0.57       | $3.0 \times 10^{-4}$  | 110                | 0.83               | 1.19                 | 1.35               | 1.12                 | 1.35               |
| B3                   | 0.115 | 0.51       | $4.0 \times 10^{-4}$  | 115                | 1.33               | 1.73                 | 2.0                | 2.13                 | 1.87               |
| B3( $\mathcal{PN}$ ) | 0.115 | 0.45       | <i>merged</i>         | 168                | 1.69               | 1.75                 | 2.10               | 2.30                 | 1.91               |
| B4                   | 0.13  | 0.48       | $3.9 \times 10^{-4}$  | 230                | 0.80               | 2.0                  | 2.9                | 3.50                 | 3.26               |
| B4( $\mathcal{PN}$ ) | 0.13  | 0.43       | <i>merged</i>         | 189                | 1.05               | 2.05                 | 2.80               | 3.34                 | 3.21               |
| C1                   | 0.066 | 0.86       | $1.25 \times 10^{-4}$ | 090                | 0.71               | 1.18                 | 1.42               | 1.51                 | 1.29               |
| C2                   | 0.066 | 0.80       | $1.2 \times 10^{-4}$  | 090                | 0.96               | 2.50                 | 2.88               | 2.60                 | 2.40               |
| C3                   | 0.067 | 0.77       | $1.4 \times 10^{-4}$  | 080                | 1.03               | 1.52                 | 2.26               | 2.40                 | 2.26               |
| C4                   | 0.069 | 0.70       | $1.02 \times 10^{-4}$ | 140                | 1.10               | 2.3                  | 3.9                | 4.80                 | 5.30               |
| D1                   | 0.045 | 1.15       | $8.3 \times 10^{-5}$  | 080                | 0.91               | 1.27                 | 1.82               | 2.01                 | 1.89               |
| D2                   | 0.046 | 1.06       | $7.1 \times 10^{-5}$  | 100                | 1.15               | 1.85                 | 2.56               | 3.04                 | 3.28               |
| D3                   | 0.046 | 1.04       | $7.0 \times 10^{-5}$  | 112                | 1.39               | 2.36                 | 3.14               | 3.81                 | 3.97               |
| D4                   | 0.047 | 1.01       | $7.9 \times 10^{-5}$  | 130                | 1.50               | 2.84                 | 3.88               | 4.96                 | 5.62               |

NOTE. — In this table the columns from left to right represent: (1) Galaxy merger model, (2) the influence radius, (3) The inner density slope  $\gamma_f$  for merger remnant, (4) the separation of the two black holes at the end of the run, (5) time at the end of the run in N-body units, (6–10) mass deficits  $M_{\text{def},n}$  in units of the mass of the binary  $M_\bullet$  measured within  $n \times r_h$ ;  $r_h$  is calculated at the time of the formation of the SMBH binary.

the evolution of the binary, and this is mostly covered in almost all of the runs. The conclusion is that the derived mass deficit is quite insensitive to the exact final time of the runs, provided this occurs at a time when the binary’s semi-major axis already reached a separation which is orders of magnitude shorter than the influence radius  $r_h$ .

Ours and the (several) observational definitions of mass deficit are obviously not equivalent, but they are surely somehow related provided the assumption that the mass is ejected by the binary holds true. We will not attempt to dwell into the intricacies of a detailed comparison, but will instead use the mass deficits obtained from our simulations as qualitative indicators regarding the evolution of the galactic nuclei as they undergo minor/major dry mergers.

The bottom panel of the Figure 6 shows the resulting mass-deficits measured out to various radii for model C1. Mass-deficits have a maximum value at around  $2-3r_h$  for each model. We are showing the value of mass-deficit at different radii in table 3 for all the runs. First, we can see that the mass-deficits are clearly larger for more concentrated (higher  $\gamma$ ) models. They are also increasing with the mass ratio  $q$ . Note that what we are directly measuring from the runs is the effect of the inspiralling binary on the stellar distribution, *not* the total amount of mass ejected by the binary. The latter value should, by simple energetic arguments and given a fixed total binary mass, be on average the same regardless of the detailed properties of the surrounding nucleus. The “damage” incurred by the stellar cusps in more concentrated nuclei, however, is expected to be greater as stars on loss cone orbits at small radii will represent a larger fraction of the (local) total stellar mass than those more outside. If galaxies undergo a series of mergers as suggested by the hierarchical galaxy formation scenario, then the mass deficits should add up because the time required to fill in the gap (removal of stars by inspiraling SMBH binary) is essentially of the order of relaxation time, which is several orders of

magnitude greater than a Hubble time for bright elliptical galaxies (Merritt 2006b). The follow up merger will redistribute the stars in phase space. The mass deficit following  $\mathcal{N}$  dry mergers is  $\mathcal{N} \cdot (M_{\text{def}}/M_\bullet)$  so the estimated mass deficits obtained from our simulations imply that at least few ( $\mathcal{N} = 2-4$ ) major mergers are required to create  $\langle M_{\text{def}}/M_\bullet \rangle \sim 11$  reported by Kormendy et al. (2009).

It is also worth pointing out that the final density profile shown the top panel of Figure 6 has a central density slope  $\gamma \sim 1$ . This means that a single inspiral is not enough to turn a steep cusp ( $\gamma \gtrsim 1.5$ ) into a core ( $\gamma \lesssim 0.5$ ).

## 5. COALESCENCE TIMES FOR SMBH BINARIES

In this section we want to derive an estimate for the coalescence times of the SMBH binaries in our simulations, similar to what has been done in Berentzen et al. (2009). In the latter work it has been shown that the predictions of coalescence times for SMBH binaries in rotating, tri-axial galactic nuclei agrees well with the results of post-Newtonian  $N$ -body simulations, up to order 2.5PN. To test the accuracy of our estimates made here, we repeat four of our  $N$ -body simulations of merging galaxies – this time including the post-Newtonian equations of motion for the SMBHs up to order 3.5PN (see Sec. 5.1).

In Fig. 2, one can see the rate of change of the binary’s inverse semi-major axis during the hard binary phase is approximately independent of time, so we can write

$$s_{\text{NB}} = -\frac{1}{a^2} \left( \frac{da}{dt} \right)_{\text{NB}} \approx \text{const.}, \quad (8)$$

a value which we can measure directly from each run.

At some time in the simulation, the semi-major axis  $a$  will have fallen to such a small value that binary shrinking due to GW emission takes over. At such small separations – depending on mass and eccentricity of the binary

– the gravitational wave emission becomes so efficient in extracting the angular momentum and energy from the binary that the latter becomes effectively decoupled from the rest of the stellar system and the SMBHs are led eventually to coalescence as if they were an isolated binary.

The orbit-averaged expressions – including the lowest order  $2.5\mathcal{PN}$  dissipative terms – for the rates of change of a binary’s semi-major axis, and eccentricity due to GW emission are given by Peters (1964):

$$\left\langle \frac{da}{dt} \right\rangle_{\text{GW}} = -\frac{64}{5} \frac{G^3 M_{\bullet 1} M_{\bullet 2} M_{\bullet}}{a^3 c^5 (1-e^2)^{7/2}} \times \left( 1 + \frac{73}{24} e^2 + \frac{37}{96} e^4 \right), \quad (9)$$

$$\left\langle \frac{de}{dt} \right\rangle_{\text{GW}} = -\frac{304}{15} e \frac{G^3 M_{\bullet 1} M_{\bullet 2} M_{\bullet}}{a^4 c^5 (1-e^2)^{5/2}} \times \left( 1 + \frac{121}{304} e^2 \right). \quad (10)$$

The corresponding hardening rate due to GW emission alone is thus given as:

$$s_{\text{GW}} = \frac{64}{5} \frac{G^3 M_{\bullet 1} M_{\bullet 2} M_{\bullet}}{a^5 c^5 (1-e^2)^{7/2}} \times \left( 1 + \frac{73}{24} e^2 + \frac{37}{96} e^4 \right), \quad (11)$$

To calculate the coalescence time in our simulations we divide the evolution into two distinct regimes (see, e.g., Preto et al. (2009)): (1) the classical regime, in which the hardening is driven by stellar-dynamical effects and (2) the relativistic regime in which the GW emission is dominant. We define this latter regime, starting from a time  $t_0$  when

$$s_{\text{NB}} = s_{\text{GW}}. \quad (12)$$

The semi-major axis  $a_0$  at time  $t_0$  can be calculated from Eq. 12 by assuming that both  $s_{\text{NB}}$  and eccentricity  $e(t)$  remain roughly constant<sup>4</sup> during the stellar dynamical hardening phase, as supported by our simulations.

We find that  $a_0$  is typically smaller than  $a_{\text{final}}$ , the semi-major axis at the time  $t_{\text{final}}$  at which our simulations end. Therefore,  $t_0$  usually exceeds  $t_{\text{final}}$  and the time interval  $\Delta t$  between  $t_{\text{final}}$  and  $t_0$  can be derived as

$$\Delta t = s_{\text{NB}}^{-1} \left( \frac{1}{a_0} - \frac{1}{a_{\text{final}}} \right). \quad (13)$$

With this, the full time to coalescence,  $t_{\text{coal}}$ , in our (Newtonian) simulations takes into account (1) the time from when the two SMBHs become gravitationally bound ( $T$ ) until they enter the GW regime  $t_0$  and (2) the binary’s lifetime  $t_{\text{GW}}$  until the final coalescence. The lifetime  $t_{\text{GW}}$  of an isolated relativistic binary can be calculated from Equations 9 and 10 for a given semi-major axis  $a_0$  and corresponding eccentricity  $e_0$ , respectively (see Eq. 5.14 in Peters 1964).

<sup>4</sup> Note that if  $e(t)$  (slightly) increases as suggested by scattering experiment by Quinlan (1996) and Paper II then the full time to coalescence shall be smaller than our estimated  $t_{\text{coal}}$ . Therefore, our results here should be interpreted as upper bounds to the true coalescence times.

In order to compute the GW evolution rates one requires to adopt some physical units, e.g., of length and mass. In paper I, we equated the effective radii of our models to the effective radii of observed galaxies to fix the mass ( $M_{\text{gal}}$ ) and the length ( $r_0$ ) units. In Paper II, we equate the influence radii of our models to that of the Galactic center and then extrapolate it to other galaxy masses by assuming the validity of the  $M_{\bullet} - \sigma$  relation and a stellar distribution  $\rho(r) \propto r^{-7/4}$  at the center. Here to compute the coalescence times, we select three different elliptical galaxies (M32, M87, NGC4486A) to scale our models to physical units (Table 4). We use the observed mass of the SMBH and its influence radius and compare it to the mass and influence radius of the primary galaxy in our models to fix  $M_{\text{gal,p}}$  and  $r_{0,p}$ . Model A’s which have a very shallow slope are scaled with M87, model B’s with NGC4486A and model D’s are scaled with M32. The choice of galaxies for our models scaling is consistent with the fact that bright ellipticals have very shallow inner slopes and faint ellipticals have steep cusps. The estimated coalescence times for SMBH binaries in our simulations obtained through the procedure described above are presented in Table 5. We find that the time interval spend in the Newtonian and in the relativistic regime, respectively, are always comparable in almost all our simulations (see column 7 in Tab. 5). This can be understood as follows: binaries with high eccentricities reach the relativistic regimes earlier than with low eccentricity and thus shortening the stellar dynamical phase. Also the higher eccentricities mean that the GW emission becomes more efficient which then shortens the relativistic inspiral phase. The black hole of M32 with a mass  $\sim 3 \times 10^6 M_{\odot}$  corresponds to possible sources detectable by LISA. The coalescence timescales for low mass black hole binaries are less than a Gyr (see table 5) which suggests that prompt coalescence of binary SMBH detectable by LISA should be very common at high redshifts. Even at the high mass end our models suggest the coalescence timescales  $\sim$  Gyr or even less depending on the eccentricity of the binary. These timescales are short enough that SMBH binaries in these galaxies should achieve full coalescence before a subsequent galaxy merger occurs. The coalescence times for SMBHs at low mass end are significantly ( $\sim 10\times$ ) shorter than the ones presented in paper I and more in line with those obtained in Paper II in which the scaling of lower-mass nuclei was set up by matching the total mass in stars to that observed in the inner  $\sim 2.5$  pc of the Galactic center. The reason for this discrepancy is the weak dependence of effective radii with galaxy luminosity relation adopted there, which was optimized for nuclei with  $\gtrsim 10^8 M_{\odot}$  black holes, but would lead to overestimate the influence radius of the Galactic center (or similarly compact nuclei) by an order of magnitude. Naturally, the coalescence times at high mass end of binary SMBHs are in nice agreement between both studies.

### 5.1. Post-Newtonian Simulations

In order to verify the accuracy of our estimate for the coalescence times given in Table 5, we select the two cases A2 and A4 from Table 5 (plus two other cases, B3 and B4, not shown) and re-started these runs with exactly same initial conditions. The choice of these runs is motivated by their relative short coalescence times compared

TABLE 4  
PHYSICAL SCALING OF OUR MODELS

| Model | Galaxy | $M_{\bullet}(M_{\odot})$ | $r_h(\text{pc})$ | $T(\text{Myr})$ | $L(\text{kpc})$ | $M(M_{\odot})$       | speed of light(c) |
|-------|--------|--------------------------|------------------|-----------------|-----------------|----------------------|-------------------|
| A     | M87    | $3.6 \times 10^9$        | 460              | 1.9             | 2.3             | $7.2 \times 10^{11}$ | 257               |
| B     | N4486A | $1.3 \times 10^7$        | 31               | 1.4             | 0.3             | $2.6 \times 10^9$    | 1550              |
| D     | M32    | $3.1 \times 10^6$        | 3                | 0.75            | 0.12            | $6.2 \times 10^8$    | 2011              |

NOTE. — Columns from left to right; (1) Primary galaxy model, (2) Observed galaxy used to scale our model, (3) Observed mass of SMBH in the galaxy in column 2, (4) observed influence radius, (5) time unit, (6) length unit, (7) mass unit and (8) speed of light in model unit.

TABLE 5  
TIME TO GRAVITATIONAL WAVE COALESCENCE

| Run | $a_{\text{final}}$   | $s_{\text{final}}$ | $e_0$ | $a_0(\text{pc})$     | $t_0(\text{Gyr})$ | $t_0/t_{\text{GW}}$ | $t_{\text{coal}}(\text{Gyr})$ |
|-----|----------------------|--------------------|-------|----------------------|-------------------|---------------------|-------------------------------|
| A1  | $6.4 \times 10^{-4}$ | 9.10               | 0.50  | $3.5 \times 10^{-1}$ | 1.30              | 2.1                 | 1.89                          |
| A2  | $5.5 \times 10^{-4}$ | 10.8               | 0.98  | $3.9 \times 10^0$    | 0.12              | 1.1                 | 0.23                          |
| A3  | $5.9 \times 10^{-4}$ | 10.3               | 0.70  | $6.9 \times 10^{-1}$ | 0.63              | 1.2                 | 1.15                          |
| A4  | $9.7 \times 10^{-4}$ | 9.60               | 0.88  | $1.6 \times 10^0$    | 0.30              | 1.1                 | 0.57                          |
| B1  | $2.9 \times 10^{-4}$ | 23.3               | 0.62  | $7.4 \times 10^{-3}$ | 2.10              | 1.3                 | 3.70                          |
| B2  | $3.0 \times 10^{-4}$ | 21.9               | 0.98  | $7.1 \times 10^{-2}$ | 0.24              | 0.5                 | 0.77                          |
| B3  | $4.0 \times 10^{-4}$ | 20.4               | 0.95  | $4.5 \times 10^{-2}$ | 0.39              | 1.4                 | 0.66                          |
| B4  | $3.9 \times 10^{-4}$ | 22.2               | 0.96  | $6.3 \times 10^{-2}$ | 0.27              | 0.7                 | 0.64                          |
| D1  | $9.2 \times 10^{-5}$ | 75.7               | 0.69  | $2.1 \times 10^{-3}$ | 0.48              | 1.0                 | 0.98                          |
| D2  | $7.1 \times 10^{-5}$ | 69.8               | 0.66  | $2.4 \times 10^{-3}$ | 0.43              | 1.0                 | 0.82                          |
| D3  | $7.6 \times 10^{-5}$ | 69.5               | 0.61  | $2.6 \times 10^{-3}$ | 0.41              | 1.4                 | 0.70                          |
| D4  | $7.5 \times 10^{-5}$ | 59.9               | 0.60  | $3.3 \times 10^{-3}$ | 0.38              | 1.3                 | 0.67                          |

NOTE. — Columns from left to right; (1) Galaxy mergers model, (2) semi-major-axis (in model units) at the end of simulation  $t_{\text{final}}$ , (3) hardening rate (model units), (4) eccentricity at  $t_{\text{final}}$ , (5) semi-major axis of the binary at which the stellar dynamical hardening becomes equal to the hardening due to GWs, (6) Life time of binary in classical stellar dynamical hardening phase, (7) ratio between the time spend in classical regime and the time spend in GW regime and (8) Full time to coalescence of SMBHs.

to other runs.

We have implemented the relativistic effects to the MBH binary only by using the  $\mathcal{PN}$  equations of motion written in the inertial frame of binary center of mass including all the terms up to  $3.5\mathcal{PN}$  order

$$\frac{d\mathbf{v}}{dt} = -\frac{GM_{\bullet}}{r^2} [(1 + \mathcal{A})\mathbf{n}_{12} + \mathcal{B}\mathbf{v}_{12}] + \mathcal{O}(1/c^8), \quad (14)$$

where  $\mathbf{n} = \mathbf{r}/r$ , the coefficients  $\mathcal{A}$  and  $\mathcal{B}$  are complicated expressions of the binary's relative separation and velocity (Blanchet 2006). The Post-Newtonian approximation is a power series expansion in  $1/c$ : the  $0^{\text{th}}$  order term corresponds to the dominant Newtonian acceleration. The  $1\mathcal{PN}$ ,  $2\mathcal{PN}$  and  $3\mathcal{PN}$  order terms are conservative and proportional to  $c^{-2}$ ,  $c^{-4}$  and  $c^{-6}$ . The dissipative  $2.5\mathcal{PN}$  and  $3.5\mathcal{PN}$  terms, which are proportional to  $c^{-5}$  and  $c^{-7}$ , cause the loss of orbital energy and of angular momentum due to the gravitational wave radiation reaction. We treat the SMBHs as point particles and thus we neglect any spin-orbit or spin-spin coupling which in general is taken into account in the  $1.5\mathcal{PN}$  (spin-orbit),  $2\mathcal{PN}$  (spin-spin) and  $2.5\mathcal{PN}$  (spin-orbit) terms in our common  $\mathcal{PN}$  implementation.

Figure 7 shows the evolution of the inverse semi-major axis  $1/a$  and eccentricity  $e$  of the SMBH binary for run A2 with and without  $\mathcal{PN}$  corrections. Hardening of the binary due to GWs emission starts to dominate at  $1/a \sim 1000$  which is slightly larger than the estimated  $1/a_0$  (all in model units). This is due to the slightly higher value of eccentricity reached during the run without  $\mathcal{PN}$  which is then used to estimate  $a_0$ . For the correct value of eccentricity obtained from run with  $\mathcal{PN}$ , the estimated  $1/a_0$  matches accurately with the value where hardening due to GWs starts to dominate. The full coalescence

time for the binary in our  $\mathcal{PN}$  simulations is 0.25 Gyr which is very close to to estimated  $t_{\text{coal}} \sim 0.23$  Gyr. The inverse semi-major axis and eccentricity evolution for model A4 are shown in figure 8. If we look at the evolution of the inverse semi-major axis for this run then we see that hardening due to GW becomes important at estimated  $1/a_0$ , as the average eccentricity evolution matches almost perfectly between the  $\mathcal{PN}$  and non- $\mathcal{PN}$  runs.

As in the (isolated) models of Berentzen et al. (2009), we find very good agreement between our estimated coalescence times and those found using full  $\mathcal{PN}$  terms in our merger runs. We should note that the coalescence times for Models D are all in the upper range of the coalescence times estimated in Paper II for  $10^6 M_{\odot}$  LISA binaries. This can be easily understood if we note that in the previous paper, the nuclei were all modeled with  $\gamma = 1$ , whereas here we choose  $\gamma = 7/4$  more in line with the expected properties of compact nuclei. We can see both from Figure 1 and Table 5 that the binary eccentricities tend to be lower ( $e \sim 0.6 - 0.65$ ) for  $\gamma = 7/4$ , and indeed in Papers I & II, the binaries reached very often values  $e \gtrsim 0.9$  (in accordance to values obtained in this paper for  $\gamma = 1$ ). The dependence on eccentricity of the coalescence time under GW emission is  $T_{\text{coal,GW}} \sim (1 - e^2)^{7/2}$  could easily account for a decrease of an order of magnitude or so when the binaries are very eccentric. It will be accordingly very important to further investigate the dependence of the eccentricity evolution under different values of  $\gamma$  and  $q$ , and this is the subject of a forthcoming paper (Preto et al. in prep.).

## 6. SUMMARY & CONCLUSIONS

Direct  $N$ -body simulation of mergers of spherically symmetric galaxies with different mass ratios were per-

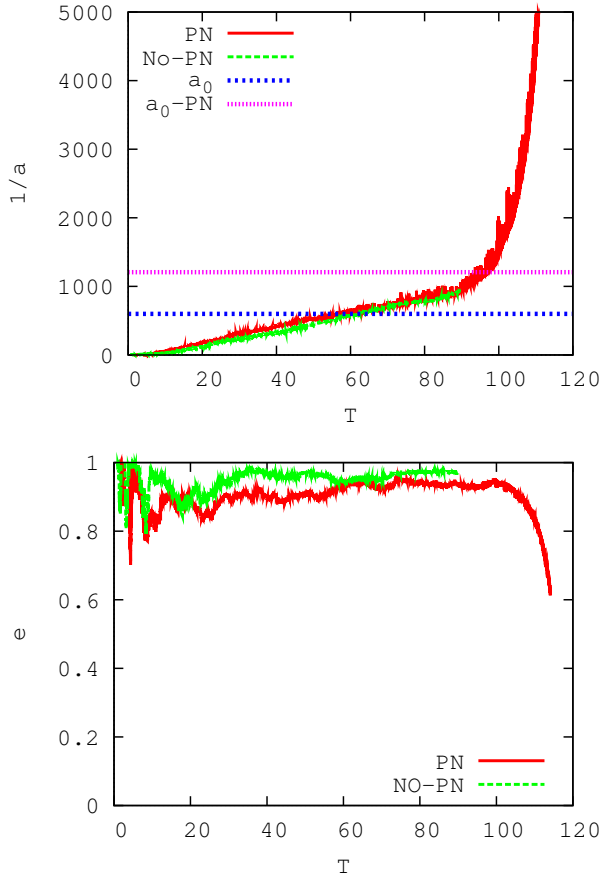


FIG. 7.— Evolution of the inverse semi-major axis  $1/a$  (top) and eccentricity  $e$  (bottom) for model A2, with and without  $\mathcal{PN}$  terms. The horizontal lines represent the estimated semi-major axis of the SMBH binary for which the stellar dynamical hardening becomes equal to the  $\mathcal{PN}$  hardening derived from the run without  $\mathcal{PN}$  ( $a_0$ ) and with  $\mathcal{PN}$  ( $a_0 - \mathcal{PN}$ ). See main text for further details.

formed to investigate the evolution of binary SMBHs from the onset of merger through the stellar hardening phase until the eventual relativistic coalescence. The merging galaxies have different initial density profiles varying from shallow ( $\gamma = 1/2, 1$ ) to steep cusps ( $\gamma = 3/2, 7/4$ ) – thus covering the range of stellar distribution typically observed in the centers of bulges or early-type galaxies. In Papers I and II, we have shown that merger-induced triaxiality could support a purely stellar dynamical solution to the FPP in the case of equal-mass mergers. In order to assess the prospects for such a solution in the more general unequal-mass case, we measured both the hardening rate and merger-induced triaxiality for mass ratios in the range  $q \in [0.05, 1]$ . The merger-induced triaxiality found in Papers I and II for equal-mass mergers is still present in unequal ( $q < 1$ ) mergers, albeit it becomes weaker as  $q$  decreases. Minor mergers with  $q \lesssim 0.05$  of spherical progenitor galaxies leave the primary almost unperturbed, so the subsequent binary evolution follows suit in an almost spherical background nucleus. The classical FPP could well show up in such cases. This transition seems to be abrupt, as the measured hardening rates are essentially independent of the mass ratio  $q$  until it suddenly declines at a value somewhere between  $q = 0.05$  and  $0.1$  – thus indicating that only a very modest triaxiality is needed for driving

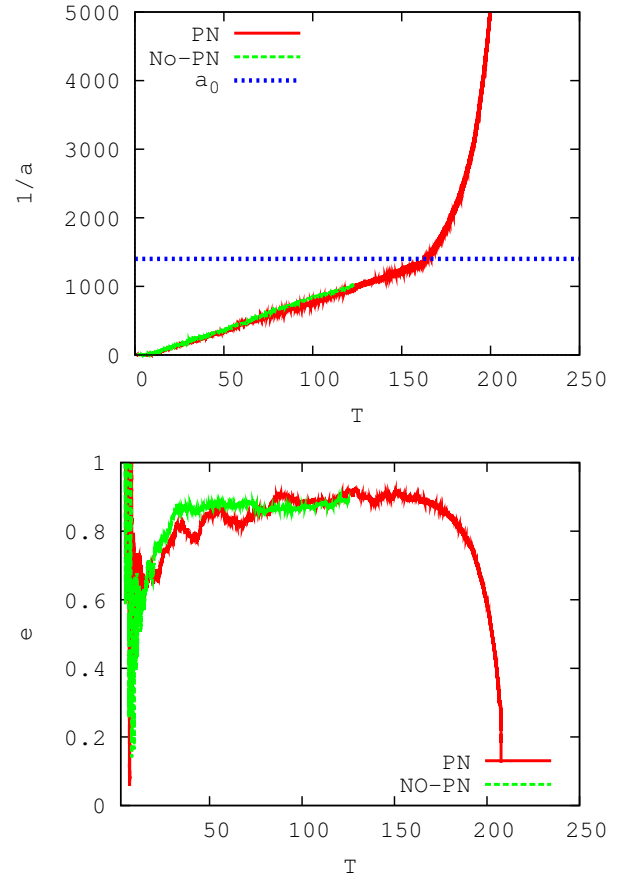


FIG. 8.— Evolution of inverse semi-major axis  $1/a$  (top) and eccentricity  $e$  (bottom) for model A4 with and without  $\mathcal{PN}$  terms.  $a_0$  is the semi-major axis of the SMBH binary for which stellar dynamical hardening is equal to  $\mathcal{PN}$  hardening.

the binary inspiral at rates consistently higher than in a spherical nucleus. It is also not surprising that we find that the hardening rate increases substantially for high  $\gamma$ , as more concentrated nuclei will have bigger amounts of centrophilic orbits.

The solution to the FPP therefore hinges strongly on the expected triaxiality – or, more precisely, the amount of centrophilic orbits supported by it – at the center of galaxy merger remnants. From this perspective, our models may represent *worst case scenarios*, since they were derived from the merger of *spherically symmetric* progenitor galaxies, which is indeed somewhat unlikely as most observed ellipticals are significantly flattened and a good fraction of them are at least mildly triaxial (Kormendy & Bender 1996; Emsellem et al. 2007). How the shape of the progenitor galaxies affects the shape of the merger remnant and the resulting SMBH hardening rates is yet unclear. Nevertheless it is important to pursue increasingly realistic stellar dynamical models of galactic nuclei in order to refine our understanding of binary SMBH evolution tracks and associated timescales. A detailed study of the  $N$ -independence and merger-induced triaxiality in unequal-mass mergers – including non-spherical progenitors resulting from previous merger events – is being currently pursued (Preto et al. in prep.).

We have produced estimates of coalescence times us-

ing a simplified prescription for the late relativistic phase of the inspiral – *i.e.* adopting the Peter’s (1964) equations for the evolution of an isolated binary and ignoring the late *stellar-driven* eccentricity evolution. We assessed the accuracy of these approximations by including Post-Newtonian terms (up to  $3.5\mathcal{PN}$  order) to the equations of motion of the binary in a few representative cases of our sample. At least in these few selected cases, the agreement is remarkably good, and this is mainly due to the fact that the eccentricity evolution is almost identical in the  $\mathcal{PN}$  and non- $\mathcal{PN}$  runs. One should add a little note of caution though. The eccentricity evolution may be a quite sensitive function of the properties of the surrounding stellar cluster (slope  $\gamma$ , mass ratio  $q$ , amount of net rotation, etc) and on the initial conditions of the binary. Previous studies indeed indicate that one could expect significant evolution of the eccentricity during the hardening phase, even though not always of the same sign (Sesana 2010; Preto et al. 2011; Sesana et al. 2011). The coalescence times resulting from our calculations are consistently shorter than a Hubble time at a given redshift (up to  $z \sim 2 - 3$  for all masses and up to  $z \sim 6 - 10$  for those in the LISA mass range). Coalescence times for binaries of  $\sim 10^6 M_\odot$  are all shorter than 1 Gyr; for the most massive  $\sim 10^9 M_\odot$  they range between hundreds of millions of years (highly eccentric ones) to  $\sim 1 - 2$  Gyr (less eccentric ones). SMBH binaries are therefore very promising sources of GWs for LISA both at low and high redshift. The coalescence times obtained here – especially those from models D – may be effectively an upper bound if the mild eccentricity growth observed in these runs is not generic (we have only four runs). In Paper II, we used models with  $\gamma = 1$  to compute the evolution of binaries in the LISA mass range and we obtained faster coalescences; this was partly because the binaries were significantly more eccentric. Therefore the detailed properties of the distribution of coalescence times hinges in part on the dependence of the eccentricity evolution on the properties of the surrounding cluster. The question of whether eccentricity grows, decays or remains approximately constant during the hardening phase remains still uncertain and we are currently pursuing it (Preto et al. in prep.). Interestingly, the duration of how long the binaries remain in the stellar dynamical hardening phase and in the relativistic one are roughly equal by an eccentricity regulated process. This means that SMBH binaries on highly eccentric orbits have less probability to be detected in the classical regime but at the same time are sources of strong GW signals to be detected. On the other hand, binaries with low eccentricities remain longer in the Newtonian regime and therefore are more likely to be observed in this phase, but may only be luminous GW sources in the final phase of coalescence.

With our results we moved another step towards a consistent stellar dynamical solution to the FPP, and thus of providing a solid dynamical substantiation to cosmological scenarios where prompt coalescences are the norm during SMBH-galaxy co-evolution (Sesana et al. 2007; Volonteri 2010). If our results hold true in real galaxies, the bottleneck to SMBH coalescences – if any – is likely to be associated to the long timescales needed for SMBHs to become a bound pair in galaxy mergers of unequal

mass – especially in case  $q \lesssim 0.1$  and gas fractions are low (Callegari et al. 2011). These results are promising for SMBH binaries being abundant LISA sources at high redshift.

What about the role of gas in hardening the SMBH binaries at sub-parsec scales? Numerical simulations of merging disk galaxies with a substantial gas-fraction have shown that gas is driven towards the central region of the merger remnant where it accumulates. As a consequence, the remnant becomes more axisymmetric (*i.e.* losing triaxiality) and the orbital structure changes noticeably as compared to the purely stellar case (Naab, Jesseit & Burkert 2006). Thus we can expect that the fraction of centrophilic orbit is affected in the same manner by the presence of the gas. In which direction it affects the hardening rate is yet an unresolved issue.

The gas which is funneled to the center of the remnant may undergo strong starbursts which may lead to the formation of a steep stellar density cusp – even before the binary has formed – as shown by Callegari et al. (2009), which then in turn increases the binary’s hardening rate as shown in this work.

The gas could certainly also assist the inspiral if it is cold enough to settle into a circumbinary thin disk (Armitage & Natarajan 2005), even though the uncertainties associated with its long-term dynamical behavior are potentially more severe than those related to stellar dynamics. For instance, gaseous disks are susceptible to fragmenting and forming stars. In order for the disk to be at worst marginally stable against fragmentation at every radius, its total mass is constrained to be  $M_{\text{disk}} \sim (0.1 - 0.2) M_\bullet$  (Cuadra et al. 2009; Lodato et al. 2009). This is not likely to be enough to drive the binary to coalescence.

The “mass deficits” induced to the centers of galaxies with no gas by inspiraling SMBH binaries are found to be of order  $\sim (1 - 5) M_\bullet$ , depending on the slope  $\gamma$  of their central stellar distribution and on their mass ratio  $q$ . This is consistent with the picture that cores in giant ellipticals are scoured by SMBH binary inspirals during successive merger events – assuming only that relaxation times are long enough in those systems for the results from different mergers to be cumulative. For galaxies in the mass range of the Milky Way the picture is basically distinct. Since the amount of mass depletion in a single merger event only partially destroys a steep inner cusp, it results that even if a major merger were to have happened in the Galactic center at redshift  $z = 1$  or larger, it would have been enough time to regrow a mass segregated Bahcall & Wolf cusp since then (Preto & Amaro-Seoane 2010).

We thank Gabor Kupa and Patrick Brem for their help in testing and implementing the  $\mathcal{PN}$  code subroutine for the binary SMBHs which we use in our phi-GRAPE+GPU code. We also thank referee for his/her valuable comments.

FK was supported by a grant from the Higher Education Commission (HEC) of Pakistan administrated by the Deutscher Akademischer Austauschdienst (DAAD). MP and RS acknowledge supported by the Deutsches Zentrum für Luft- und Raumfahrt (through LISA Germany project). We acknowledge support by the Chinese

Academy of Sciences Visiting Professorship for Senior International Scientists, grant number 2009S1-5 (The Silk Road Project; R.S. and P.B.). PB and IB both acknowledge financial support by the Deutsche Forschungsgemeinschaft (DFG) through SFB 881 "The Milky Way System" (sub-projects Z2 and A1) at the Ruprecht-Karls-Universität Heidelberg.

PB acknowledges the special support by the NASU under the Main Astronomical Observatory GRID/GPU computing cluster project ("graffias" cluster). PB's studies are also partially supported by the program Cosmophysics of NASU.

IB acknowledges funding through a Frontier Innovation

grant of the University of Heidelberg sponsored by the German Excellence Initiative.

We used following GPU cluster to run our simulations. "laohu" at the Center of Information and Computing at National Astronomical Observatories, Chinese Academy of Sciences, funded by Ministry of Finance of People's Republic of China under the grant ZDYZ2008-2. "kolob" which has been funded through a Frontier project supported by the excellence scheme of the University of Heidelberg and by the DFG. "titan", funded under the grants I/80 041-043 and I/81 396 of the Volkswagen Foundation and grants 823.219-439/30 and /36 of the Ministry of Science, Research and the Arts of Baden-Württemberg, Germany.

## REFERENCES

- Alexander, T., & Hopman, C. 2009, *ApJ*, 697, 1861  
 Armitage, P. & Natarajan, P. 2005, *ApJ*, 634, 921  
 Bahcall, J. N., & Wolf, R. A. 1976, *ApJ*, 209, 214  
 Bahcall, J. N., & Wolf, R. A. 1977, *ApJ*, 216, 883  
 Barack, L., & Cutler, C. 2004, *Physical Review D*, 69, 082005  
 Begelman, M. C., Blandford, R. D., & Rees, M. J. 1980, *Nature*, 287, 307  
 Berczik, P., Merritt, D., & Spurzem, R. 2005, *ApJ*, 633, 680  
 Berczik, P., Merritt, D., Spurzem, R., Bischof, H., 2006, *ApJ*, 642, L21  
 Berentzen, I., Preto, M., Berczik, P., Merritt, D., & Spurzem, R. 2009, *ApJ*, 695, 455  
 Binney, J. & Tremaine, S. 2008, *Galactic Dynamics* (Princeton, NJ, Princeton University Press, 2008)  
 Blanchet, L., 2006, *Living Rev. Relativity*, 9, 4.<sup>5</sup>  
 Buchholz, R., Schödel, R., & Eckart, A. 2009, *A&A*, 499, 483  
 Callegari, S., Mayer, L., Kazantzidis, S., Colpi, M., Governato, F., Quinn, T., & Wadsley, J. 2009, *ApJ*, 696, L89  
 Callegari, S., Kazantzidis, S., Mayer, L., Colpi, M., Bellovary, J. M., Quinn, T., & Wadsley, J. 2011, *ApJ*, 729, 85  
 Cuadra, J., Armitage, P. J., Alexander, R. D., & Begelman, M. C. 2009, *MNRAS*, 393, 1423  
 Danzmann, K. *et al.*, 2011, *ESA LISA Yellow Book*<sup>6</sup>  
 Dehnen W., 1993, *MNRAS*, 265, 250  
 Do, T., Ghez, A. M., Morris, M. R., Lu, J. R., Matthews, Keith and Yelda, S., & Larkin, J. 2009, *ApJ*, 703, 1323  
 Emsellem, E., Cappellari, M., Krajnović, D., van de Ven, G., Bacon, R., Bureau, M., Davies, R. L., de Zeeuw, P. T., Falcón-Barroso, J., Kuntschner, H., McDermid, R., Peletier, R. F., Sarzi, M., 2007, *MNRAS*, 379, 401  
 Faber, S. M., Tremaine, S., Ajhar, E. A., Byun, Y.-I., Dressler, A., Gebhardt, K., Grillmair, C., Kormendy, J., Lauer, T. R. and Richstone, D. 1997, *AJ*, 114, 1771  
 Ferrarese, L., & Merritt, D. 2000, *ApJ*, 539, L9  
 Ferrarese, L., & Ford, H. 2005, *Space Science Reviews*, 116, 523  
 Ferrarese, L., *et al.* 2006, *ApJS*, 164, 334  
 Gebhardt *et al.*, 2000, *ApJ*, 539, L13  
 Gaburov E., Harfst S., Portegies Zwart S., 2009, *New Astron.*, 14, 630  
 Graham, A. W., 2004, *ApJ*, 613, L33  
 Gualandris A. & Merritt D. 2008, *ApJ*, 678, 780  
 Gualandris A. & Merritt D. 2012, 744, 74  
 Harfst, S., Gualandris, M., Merritt D., Spurzem, Portegies Zwart S., Berczik P., 2007, *NewA*, 12, 357  
 Häring, N., & Rix, H. 2004, *ApJ*, 604, 89  
 Hopkins, P.F., Cox, T.J., Dutta, S.N., Hernquist, L., Kormendy, J., Lauer, T.R., 2009, *ApJS*, 181, 135  
 Hopkins, P.F., Lauer, T.R., Cox, T.J., Hernquist, L., Kormendy, J., 2009, *ApJS*, 181, 486  
 Hughes, S. A. 2003, *Annals of Physics*, 303, 142  
 Kazantzidis, S. 2010, in *ASP Conf. Ser.* 424, *Coevolution of Galaxies and Supermassive Black Holes: A Key to Fundamental Physics and Galaxy Formation*, ed. K. Tsinganos, D. Hatzidimitriou, & T. Matsakos (San Francisco: ASP), 367  
 Khan, F. M., Just, A., & Merritt, D. 2011, *ApJ*, 732, 89  
 Komossa, S. 2006, *Memorie della Societ Astronomica Italiana*, 77, 733  
 Kormendy, J., & Bender, R. 1996, *ApJ*, 464, 119  
 Kormendy, J., Fisher D.B., Cornell M. E., & Bender, R. 2009, *ApJS*, 182, 216  
 Lightman, A. P. & Shapiro, S. L. 1977, *ApJ*, 211, 244  
 Lodato, G., Nayakshin, S., King, A. R. & Pringle, J. E., 2009, *MNRAS*, 398, 1392  
 Makino, J., & Ebisuzaki, T. 1996, *ApJ*, 465, 527  
 Makino, J., & Funato, Y. 2004, *ApJ*, 602, 93  
 Merritt, D. & Ferrarese, L. 2001, *MNRAS*, 320, L30  
 Merritt, D. & Ekers, R. D. 2002, *Science*, 297, 1310  
 Merritt, D., & Poon, M. Y. 2004, *ApJ*, 606, 788  
 Merritt, D., & Milosavljević, M. 2005, *Living Reviews in Relativity*, 8, 8  
 Merritt, D. 2006, *ApJ*, 648, 976  
 Merritt, D. 2006, *Reports on Progress in Physics*, 69, 2513  
 Merritt, D., Mikkola, S., Szell, A. 2007, *ApJ*, 671, 53  
 Merritt, D. 2009, *ApJ*, 694, 959  
 Merritt, D. 2010, *ApJ*, 718, 739  
 Merritt, D., & Vasiliev, E. 2011, *ApJ*, 726, 61  
 Milosavljević, M., & Merritt, D., Rest, A., & van den Bosch, F. C. 2002, *MNRAS*, 331, L51  
 Milosavljević, M., & Merritt, D. 2003, *ApJ*, 596, 860  
 Mikkola, S., Aarseth, S. 1998, *New Astronomy*, 3, 309  
 Naab, T., Jesseit, R., Burkert, A., 2006, *MNRAS*, 372, 839  
 Perets, H. B., & Alexander, T. 2008, *ApJ*, 677, 146  
 Peters, P. C. 1964, *Phys. Rev. B*, 136, 1224  
 Poon, M. Y., & Merritt, D. 2001, *ApJ*, 549, 192  
 Preto, M., Merritt, D., & Spurzem, R. 2004, *ApJ*, 613, L109  
 Preto, M. & Amaro-Seoane, P. 2010, *ApJ*, 708, L42  
 Preto, M., Berentzen, I. Berczik, P., Merritt, D. & Spurzem, R. 2009, *Journal of Physics: Conference Series*, Volume 154, Issue 1, pp. 012049  
 Preto, M., Berentzen, I. Berczik, P., & Spurzem, R. 2011, *ApJ*, 732, L26  
 Preto, M., Khan, F. M., Berentzen, I., Berczik, P., Just, A. & Spurzem, R., *in preparation*  
 Quinlan, G. D. 1996, *New Astron.*, 1, 35  
 Rhook, K. J., & Wyithe, J. S. B. 2005, *MNRAS*, 361, 1145  
 Roos, N. 1983, Kaastra, J. S., & Hummel, C. A 1993, *ApJ*, 409, 130  
 Sesana, A. 2010, *ApJ*, 719, 851  
 Sesana, A., Volonteri, M. & Haardt, F. 2007, *MNRAS*, 377, 1711  
 Sesana, A., Gualandris, A. & Dotti, M. 2011, *MNRAS*, 415, L35  
 Sridhar, S., & Tuma, J. 1999, *MNRAS*, 303, 483  
 Spitzer, L. 1987, *Dynamical evolution of globular clusters*, (Princeton, NJ, Princeton University Press)  
 Valtonen, M. J. *et al.* 2008, *Nature*, 451, 452  
 Volonteri, M., Haardt, F. & Madau, P. 2003, *ApJ*, 582, 559  
 Volonteri, M. 2010, *A&A Rev.*, 18, 279  
 Yu, Q. 2002, *MNRAS*, 331, 935

<sup>5</sup> URL (cited on June 2007):<http://www.livingreviews.org/lrr-2006-4>

<sup>6</sup> URL (cited on August 2011):<http://sci.esa.int/science-e/www/object/index.c>